Growth and properties of strained VO_x thin films with controlled stoichiometry

A. D. Rata,[1] A. R. Chezan,[2] M. W. Haverkort,[3] H. H. Hsieh,[4] H.-J. Lin,[4] C. T. Chen,[4] L. H. Tjeng,[3] and T. Hibma[1]
[1]*Chemical Physics, Materials Science Centre, Rijksuniversiteit Groningen, Nijenborgh 4, Groningen 9747 AG, The Netherlands*
[2]*Nuclear Solid State Physics, Materials Science Centre, Rijksuniversiteit Groningen, Nijenborgh 4, Groningen 9747 AG, The Netherlands*
[3]*II. Physikalisches Institut, Universität zu Köln, Zülpicher Strasse 77, 50937 Köln, Germany*
[4]*Synchrotron Radiation Research Center, Hsinchu 30077, Taiwan*
(Received 5 December 2002; revised manuscript received 27 May 2003; published 13 February 2004)

We have succeeded in growing epitaxial films of rocksalt VO_x on MgO(001) substrates. The oxygen content as a function of oxygen flux was determined using $^{18}O_2$-Rutherford backscattering spectrometry and the vanadium valence using x-ray-absorption spectroscopy. The upper and lower stoichiometry limits found are similar to those known for bulk material ($0.8<x<1.3$). From the reflection high-energy electron diffraction oscillation period a large number of vacancies for both vanadium and oxygen were deduced, i.e., $\approx 16\%$ for stoichiometric VO. These numbers are, surprisingly, very similar to those for bulk material and consequently quite strain insensitive. X-ray-absorption spectroscopy measurements reveal that the vacancies give rise to strong non-cubic crystal field effects. The electrical conductivity of the films is much lower than the conductivity of bulk samples, which we attribute to a decrease in the direct overlap between t_{2g} orbitals in the coherently strained layers. The temperature dependence of the conductivity is consistent with a variable range hopping mechanism.

DOI: 10.1103/PhysRevB.69.075404 PACS number(s): 68.55.−a, 81.15.Hi, 78.70.Dm, 73.61.Le

I. INTRODUCTION

One of the major challenges in transition-metal oxide thin-film research is to grow the material in single-crystal form with controlled oxygen stoichiometry. This is not a trivial task, especially when the transition-metal ion has multiple valences and the variation of the oxygen content leads to rich and complex phase diagrams. Important examples of such materials include the binary oxide systems such as the vanadium and titanium oxides.[1–5] The most common and convenient growth methods in thin-film research such as pulsed laser deposition and sputtering techniques are not very suitable here, because of the high substrate temperatures and consequently also high oxygen pressures usually used, giving less opportunity to fine tune the oxygen stoichiometry. These techniques are obviously the method of choice for ternary and quaternary oxides, where one can vary the material properties by tuning one of the constituent cation concentrations while keeping that of the oxygen fixed. For the binary oxides, however, one has to resort to true molecular-beam-epitaxy (MBE) techniques, in which one has to carefully balance the oxygen flux with respect to the metal evaporation rates in order to obtain good control and tuning of the stoichiometry. The question here is whether one can obtain thin films with physical properties that are systematic, controllable, and tunable.

Here we report on our research project to grow single-crystal thin films of vanadium monoxide (VO_x), as well as on the study of the physical properties and the electronic structure of these films. Bulk vanadium monoxide has many intriguing properties that are closely related to the issue of stoichiometry. While at first sight the crystal seems to have a simple fcc rocksalt structure, it actually can have a very wide range of varying oxygen concentrations: values of x between 0.8 and 1.3 have been reported for bulk VO_x. Even more remarkable is the large number of both cation and anion vacancies, even for $x=1$, in which case the concentrations are as high as 15%.[6] Stoichiometric VO always remains disordered, whereas ordering of the vacancies was only reported for x between 1.2 and 1.3.[7] A systematic investigation of the physical properties of polycrystalline VO_x has been carried out by Banus *et al.*[6] in the early 1970's. VO_x shows an interesting transition from a metallic to a semiconducting behavior at x close to 1, and the magnetic susceptibility can be described by a Curie-Weiss law, suggesting that the V $3d$ electrons partially localize.[3] Several models have been proposed to explain these properties, where the role of electron correlation effects, band formation, and vacancies are discussed.[8–11]

Only very little work on films of VO_x has been done till now. Metal-supported vanadium oxides were investigated by a number of authors in connection with catalytic properties. Thin vanadium layers deposited on Cu(100) (Refs. 12 and 13) and Ni(110) (Ref. 14) were found to consist of a V_2O_3-like phase after room-temperature oxidation. Growth of VO_x-like island was reported on Rh(111).[15] Surnev and co-workers[16,17] found a VO/VO_2-like phase at low coverage on Pd(111) using scanning tunnelling microscopy. Sambi and co-workers[19–21] studied thin films of VO_x on TiO_2 substrates motivated by the enhanced catalytic activity shown by titania-supported vanadium oxides.[18] Locally ordered VO_x films with a thickness up to 4 monolayers (ML) were grown on $TiO_2(110)$ by evaporating metallic vanadium at room temperature and subsequent annealing in vacuum for a short period of time, in order to promote the uptake of oxygen from the substrate. From a structural point of view, local order of their films is supported by x-ray photoelectron diffraction.

In the examples mentioned above, the vanadium oxidation state was established on the basis of the position and shape

of the V $2p_{3/2}$ photoemission line. However, the uncertainty of stoichiometry of vanadium films remains, since the binding energies of the V $2p_{3/2}$ peak for different oxidation states are very close. A comparison between data obtained in Refs. 12 and 19 shows some discrepancies. Moreover, an analysis of the physical properties of the VO_x thin films is missing in these studies. Preparation is often found to be difficult since VO_x easily oxidizes to V_2O_3. This problem can be avoided by growing epitaxial films of VO_x on appropriate substrates with a careful optimization of the evaporation conditions.

This paper describes how we have successfully grown coherent epitaxial single crystalline VO_x thin films by stabilizing them on MgO(100) substrates. The paper is organized as follows. The details of the experimental conditions and equipment used are presented in Sec. II. The results are described in Sec. III. We first present (Sec. III A) the growth process as monitored structurally *in situ* by reflection high-energy electron diffraction (RHEED) and low-energy electron diffraction (LEED) and compositionally by x-ray-photoelectron spectroscopy (XPS). We determine (Sec. III B) the stoichiometry x of the various VO_x films by using Rutherford backscattering spectrometry (RBS). Further structural details of the epitaxy are revealed by *ex situ* x-ray diffraction (XRD) in Sec. III C. The important issue of vacancy concentrations is addressed using a combination of RBS data and RHEED intensity oscillations in Sec. III D. Basic data about the electronic structure, such as the valence and local crystal fields of the ions (Sec. III E), are measured using soft-x-ray-absorption spectroscopy (XAS). We end the Results section by presenting the temperature-dependent transport properties of the films (Sec. III F). Finally we discuss the results by comparing the properties of the VO_x thin films with those of the bulk material and with predictions of existing theoretical models.

II. EXPERIMENT

The experiments were performed in an ultrahigh vacuum (UHV) MBE system, with a base pressure below 1×10^{-10} mbar. The system is equipped with RHEED, LEED, and XPS facilities. RBS and XRD were used to characterize the thin films grown in the MBE system *ex situ*. We chose MgO(100) as substrate, because it has the same cubic rock-salt structure as VO_x with a mismatch of about 3%. MgO blocks were cleaved *ex situ* and immediately introduced into the UHV chamber. The substrates were further cleaned by annealing at 650 °C for 2 h in 1×10^{-6} mbar oxygen to remove hydrocarbon contamination. Clean and well-ordered surfaces were obtained, as determined by XPS, RHEED, and LEED. High-purity vanadium (V) (99.99%) was evaporated using an electron-beam evaporator (Omicron EFM3). The deposition rate of V, measured by moving a quartz crystal at the position of the substrate, was set to 0.7–0.8 Å/min. Vanadium was simultaneously oxidized by a beam of $^{18}O_2$ (99.99%). Oxygen was supplied through a leak valve into a small buffer volume[22] connected to the vacuum chamber through a 35-cm-long and 1-cm-wide stainless steel pipe, ending at a distance of 10 cm from the substrate. The pressure in the buffer volume was monitored with a Baratron capacitance manometer. The variation in buffer pressure during deposition was less than 1%. VO_x films with different stoichiometries were grown by varying the $^{18}O_2$ buffer volume pressure, while keeping the V flux constant. During evaporation the background pressure was 2×10^{-8} mbar or lower. The V and $^{18}O_2$ beams can be abruptly and simultaneously stopped. After closing the $^{18}O_2$ valve, the background pressure dropped to below 10^{-9} mbar within seconds, ensuring a well-defined oxygen exposure of the sample. All the samples were grown while keeping the substrate at room temperature.

RHEED can be used during growth to monitor the evolution of the films. Thicknesses were calibrated by monitoring the RHEED intensity oscillations during deposition. Oscillations in the RHEED specular beam intensity, where each oscillation corresponds to the formation of one new atomic ML, allows for control of the film thickness. Film thicknesses were also determined *ex situ* from x-ray specular reflectivity measurements[23,24] and good agreement with RHEED intensity oscillations was obtained.

XPS measurements were performed using nonmonochromatic Al $K\alpha$ radiation ($h\nu=1486.6$ eV). The total energy resolution of the electron analyzer in combination with the photon source was about 1 eV. To avoid *ex situ* postoxidation, a thin MgO cap layer (20 Å) was grown for protection by Mg deposition in $^{18}O_2$ atmosphere of 1×10^{-8} mbar at room temperature. All the *ex situ* measurements, i.e., RBS, XRD, XAS, and electrical measurements, were thus performed on capped VO_x samples.

The oxygen content was determined by RBS measurements. For calibration purposes a V_2O_3 epitaxial thin film was also grown on an $Al_2O_3(0001)$ substrate, with the oxygen partial pressure and the substrate temperature set at 10^{-6} mbar and 550 °C, respectively.[25–27] All the measurements were done in a so-called ''random'' orientation with respect to the crystalline axes, using a He^+ beam with 1.5 MeV energy. The backscattering yields were detected at an angle of 165 deg.

The XRD measurements were carried on using a Philips MRD diffractometer, equipped with a hybrid mirror/monochromator for Cu K_α radiation, a four-circle goniometer and a programmable slit in front of the detector.

The XAS measurements were performed at the 11 A Dragon beamline[28,29] at the Synchrotron Radiation Research Center Taiwan, using the total electron yield mode. The light has a degree of linear polarization of 98% and an energy resolution of 0.16 eV for photon energies between 500 and 550 eV. The spectra are normalized to the photon flux measured using a gold mesh. The angle of the incident light is normal to the VO_x films.

Resistivity measurements were performed in a commercial quantum design PPMS system, in the constant voltage mode. The current was measured along the [100] direction of the films by two- and four-point geometry. Electrical contacts consisting of 10 nm of Cr metal were evaporated *ex situ* on the MgO substrates prior to introduction into the MBE system, in order to measure the resistance of as-grown VO_x films.

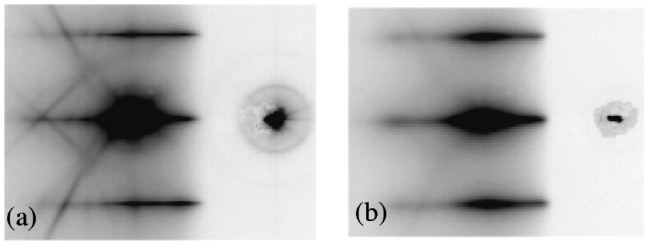

FIG. 1. RHEED patterns recorded at an electron energy of 15 kV with the beam incident along the [100] direction. (a) Clean MgO(100) substrate. (b) 20-Å VO_x(100) thin film grown on MgO(100) substrate using 0.18 mTorr oxygen buffer pressure while keeping the substrate at room temperature. The picture is inverted in order to observe better the Kikuchi lines.

III. RESULTS

A. Growth of VO_x thin films

For a wide range of incident oxygen fluxes, epitaxial growth of VO_x thin films on MgO(100) substrates was concluded from *in situ* RHEED and LEED analyses. The geometry of the MBE system allows for monitoring changes in surface structure during film growth by RHEED. This low-angle electron-diffraction technique is particularly suited to thin-film growth as it is highly sensitive to surface morphology. A RHEED pattern of a clean MgO(100) surface and 20 Å-thick VO_x thin film deposited on MgO(100) is shown in Fig. 1. The beam was incident along the [100] direction. The basic RHEED pattern did not change during growth, indicating that the film continues to grow as a rocksalt phase on top of the underlying substrate. Sharp streaks and the presence of Kikuchi lines indicate that the surface is still smooth after deposition of 10 ML of VO_x.

In most cases oscillations in the intensity of the specularly reflected beam were observed during growth. These oscillations are characteristic of a *layer-by-layer* growth mode; each oscillation corresponding to the formation of one atomic layer. Note that RHEED oscillations were observed at room temperature, which is considered to be a very low temperature for an oxide system.[30] In Fig. 2 an example of these growth oscillations is shown.

A sequence of RHEED patterns which were taken after deposition of about 50 ML of VO_x using different oxygen fluxes, is presented in Fig. 3. The oxygen content x is indicated on each RHEED pattern. The corresponding oxygen flux used can be found in the caption of Fig. 3. We will explain in Sec. III B how the x values were determined using RBS spectrometry. Varying the oxygen buffer pressure between 0.12 and 0.20 mTorr ($0.82<x<0.97$) epitaxial growth is obtained and sharp streaks can still be observed after deposition of 50 ML VO_x. The distance between VO_x streaks is the same as between the MgO streaks. This is consistent with coherent growth as determined *ex situ* by XRD, which will be discussed in Sec. III C. The rocksalt structure of VO_x thin films was also confirmed by LEED. The LEED pattern displays the same square symmetry and periodicity as a MgO(100) surface.

Between 0.22 and 0.30 mTorr, i.e., $1.1<x<1.31$, MgO RHEED streaks fade away quickly after starting the growth and three-dimensional transmission spots appear, suggesting considerable roughening of the surface. The absence of a LEED pattern for the $x=1.28$ and $x=1.31$ cases confirms that the surface morphology is becoming increasingly disordered above 1.28. Nevertheless, the presence of RHEED oscillations shows that the growth still is *layer-by-layer*-like.

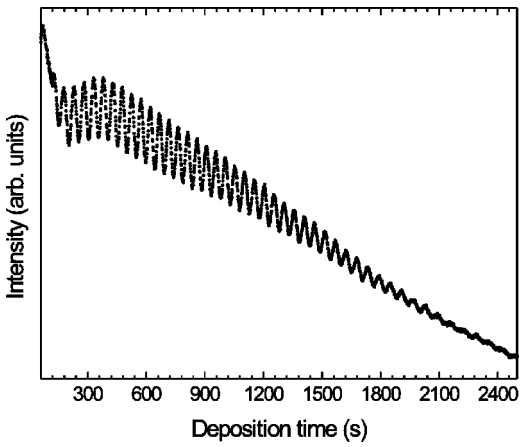

FIG. 2. RHEED intensity oscillations of the specularly reflected electron beam observed during deposition of VO_x on MgO(100). The electron beam was incident along the [100] direction, with a primary energy of 15 kV.

For an oxygen buffer pressure of less than 0.12 mTorr ($x<0.8$) powder rings and extra spots were observed in RHEED. Vanadium atoms are not completely oxidized in the latter case as deduced from XPS core-level intensities.

We mention that attempts to make VO_x films at higher substrate temperatures were unsuccessful. The RHEED pattern quickly disappeared or became very diffuse from the beginning of the growth.

The V $2p$ and O $1s$ core lines measured for three different films, i.e., vanadium metal on MgO(100), VO_x on MgO(100), and V_2O_3 on Al_2O_3(0001), are shown in Fig. 4. The binding energies were corrected for the charging effect by assuming a constant binding energy of the O $1s$ peak at 531 eV. All spectra were corrected in a standard manner for the satellites due to the $K\alpha_3\alpha_4$ components of the incident x ray and an integral background was subtracted afterwards. The binding energies of the V $2p_{3/2}$ peaks found are given in the figure. The binding energy corresponding to the V $2p_{3/2}$ in the VO_x film was found between those corresponding to V metal and V_2O_3, respectively (see Fig. 4). The vanadium oxidation state can be in principle determined from the position and shape of the V $2p_{3/2}$ feature. Nevertheless, because to different vanadium oxidation states correspond rather similar values for the $2p_{3/2}$ binding energies,[31] we did not perform a quantitative analysis of the XPS data. In order to determine precisely the stoichiometry we have adopted a different route, which will be presented in the following section.

B. Stoichiometry determination

The oxygen content of the films was determined from RBS measurements. As already mentioned in the experimen-

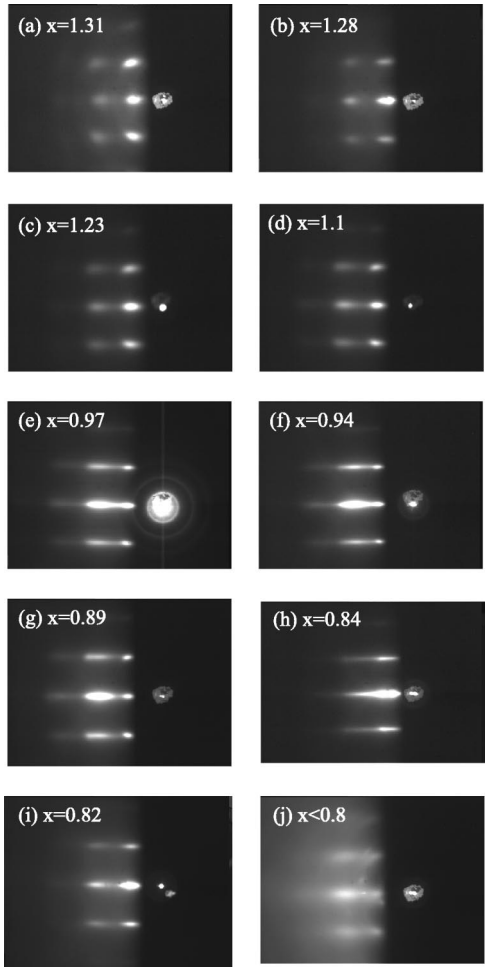

FIG. 3. Sequence of RHEED patterns observed after deposition of 50-ML VO_x on MgO(100) at different oxygen fluxes while keeping the substrate at room temperature. The oxygen buffer pressure was varied between 0.10 and 0.30 mTorr: (a) 0.30 mTorr, (b) 0.27 mTorr, (c) 0.24 mTorr, (d) 0.22 mTorr, (e) 0.20 mTorr, (f) 0.18 mTorr, (g) 0.16 mTorr, (h) 0.14 mTorr, (i) 0.12 mTorr, (j) 0.10 mTorr. The electron beam was incident along the [100] direction, with a primary energy of 15 kV.

tal part, $^{18}O_2$ instead of $^{16}O_2$ was employed for film growth in order to distinguish between the oxygen peaks corresponding to the film and the substrate, respectively. The use of a 1.5-MeV He^+ beam ensures a good mass separation between ^{16}O and ^{18}O species. This can be observed in Fig. 5, showing the RBS spectrum of a V_2O_3 layer grown epitaxially on an $Al_2O_3(0001)$ substrate that was used for calibration. A nice hexagonal LEED pattern characteristic of the corundum structure was observed, proving the high quality and long-range order of the V_2O_3 film. We plot in Fig. 6 part of the spectra for capped and uncapped VO_x layers on MgO(001) substrates. In both spectra a well-separated ^{18}O-peak is visible. For the uncapped layer, an additional shoulder at the ^{16}O position can be observed due to the fact that the layer is postoxidized in air. The absence of this shoulder in the spectrum of the capped layer proves that capped VO_x films are indeed protected from postoxidation.

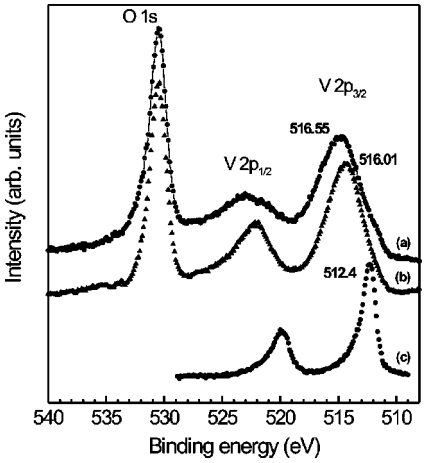

FIG. 4. V $2p$ and O $1s$ XPS spectra of (a) V_2O_3 on Al_2O_3 (0001), (b) VO_x on MgO(001), and (c) vanadium metal on MgO(001).

We calculated the O/V ratio in VO_x films with the following relation, using V_2O_3 as a reference sample:

$$x = \frac{3}{2}\frac{\left[\frac{A_O}{A_V}\right]_{VO_x}}{\left[\frac{A_O}{A_V}\right]_{V_2O_3}}. \quad (1)$$

The areas of the oxygen and vanadium peaks (A_O, A_V) in the RBS spectra were determined by fitting the V and ^{18}O peaks from VO_x and V_2O_3 samples to a Gaussian function, in the case of the ^{18}O peak after subtraction of the linear background due to Mg. The ^{18}O-peak area was corrected for the contribution of the cap layer, using the thickness of the VO_x films and the $Mg^{18}O$ cap layer as determined from the RHEED oscillations. The resulting x values are plotted in Fig. 7 as a function of the oxygen buffer volume pressure for two series of samples. One can observe that the x values are nicely reproducible. The error in the determination is about 3%. The upper and lower stoichiometry limits are similar to those known for bulk material. For the $x=0.45$ sample, XPS

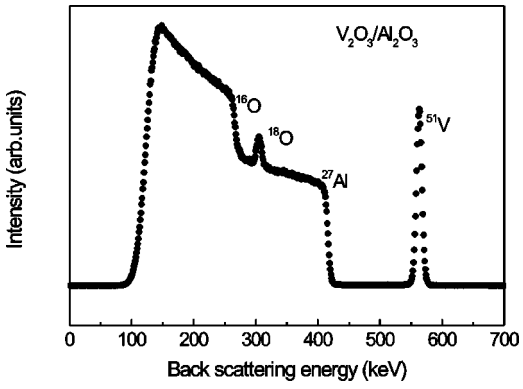

FIG. 5. RBS spectra of 1.5 MeV He^+ ions scattered from a V_2O_3 film epitaxially grown on an $Al_2O_3(0001)$ substrate. The ^{18}O peak can be clearly distinguished.

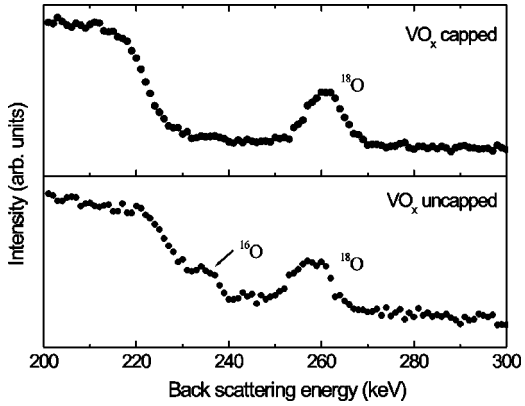

FIG. 6. RBS spectra of 1.5 MeV He^+ ions scattered from VO_x film deposited on MgO(100). (a) with a thin (2 nm) MgO cap layer, (b) without cap layer. An extra ^{16}O feature is observed due to postoxidation in the later case.

measurements indicate that vanadium is not completely oxidized. For x bigger than 1.3 a mixture of two phases was found.

C. Structure of VO_x thin films

As discussed in the preceding section, the RHEED and LEED experiments indicate that the VO_x films grow epitaxially on MgO(100). To analyze the epitaxy and crystal structure of the films in a more quantitative way, we also performed *ex situ* XRD analysis. The measurements were done on samples capped with a thin (20 Å) epitaxial MgO film. $\theta-2\theta$ scans show only weak diffraction peaks close to the (002) and (004) peaks of the MgO substrate, as expected from films having a rocksalt structure. The reflections are broadened due to the finite thickness of the film. There are no peaks corresponding to other phases. Moreover, for samples made with the oxygen buffer pressure varying between 0.12 and 0.22 mTorr a number of subsidiary thickness fringes were observed, indicating a well defined composition and thickness of the film (see Fig. 8).

To determine whether the growth is fully coherent or partially relaxed, the most convenient way is to measure the

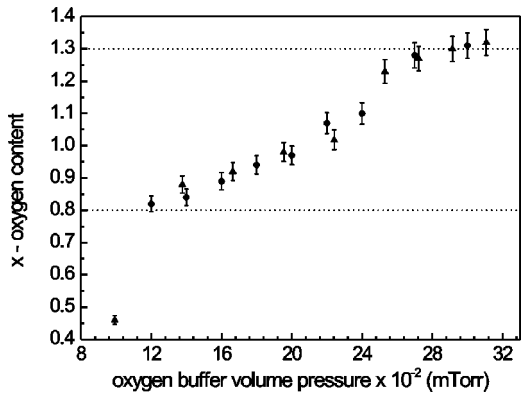

FIG. 7. The oxygen content x as function of the buffer volume pressure as determined from RBS data for two series of VO_x samples.

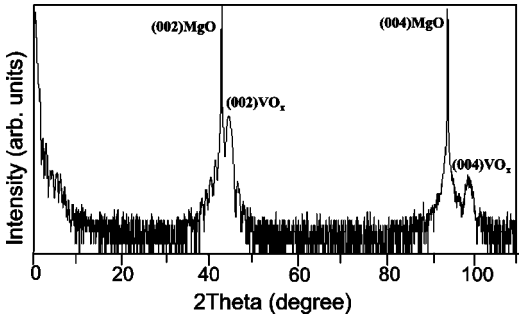

FIG. 8. $\theta-2\theta$ x-ray-diffraction measurement of a 10-nm-thick VO_x thin film prepared with $x=0.94$. Only the (002) and (004) diffraction peaks characteristic of the rocksalt structure can be observed. The reflections from the film are broadened due to the finite thickness of the film. Subsidiary thickness fringes indicate a well-defined composition and thickness of the film.

intensity profile around a nonspecular reflection common to the substrate and the overlayer. This can be obtained by performing a set of $2\theta-\omega$ scans at different ω, 2θ and ω being the detector and sample orientations with respect to the beam direction. These scans can be easily mapped into reciprocal space. An example of such mapping for the region in reciprocal space around the (113) reflection is shown in Fig. 9. The horizontal and vertical axes are k vectors parallel ($k_\parallel$) and perpendicular ($k_\perp$) to the surface plane, respectively. The intensity scale in the figure is logarithmic. The feature corresponding to the VO_x film can be clearly distinguished. The elongated shape of the MgO reflection perpendicular to the radial direction is due to mosaic spread. The peaks of MgO and VO_x are at the same $k_\parallel$ value, which proves that the film is fully coherent. Consequently, VO_x thin films experience a compressive strain in the perpendicular direction, which is induced by the lattice mismatch.

The lattice constant normal to the substrate surface can be determined from $\theta-2\theta$ scans around MgO(002) or

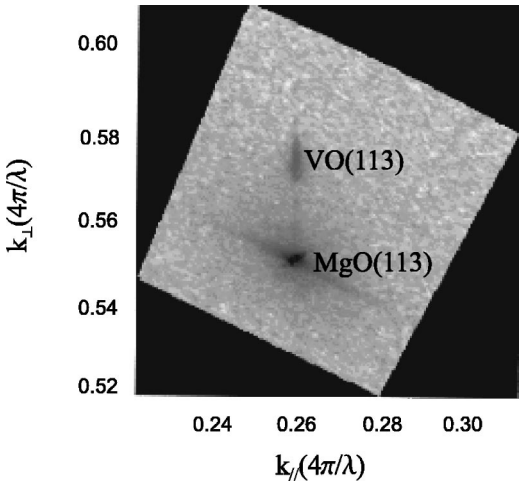

FIG. 9. XRD map of reciprocal space around the nonspecular (113) reflection of a 10-nm-thick VO_x thin film with $x=0.94$. The logarithm of the diffracted intensity as a function of the in-plane $k_\parallel$ and out-of-plane $k_\perp$ reciprocal lattice vectors is plotted. The x and y axes are in units of $4\pi/\lambda$, with $\lambda=0.150\,15$ nm.

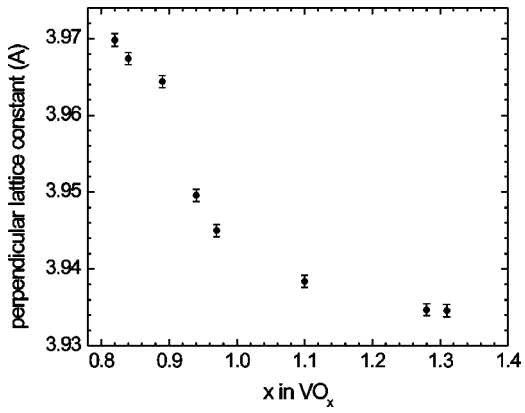

FIG. 10. Perpendicular lattice constant of VO_x films with different oxygen content as a function of x as determined from XRD. The perpendicular lattice constant is decreasing with increasing x.

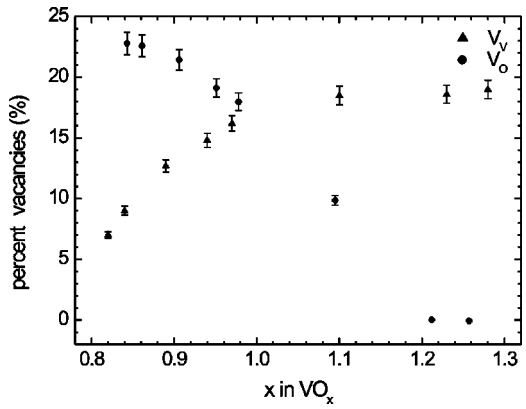

FIG. 11. Vanadium and oxygen vacancy concentrations in VO_x as determined from the period of RHEED oscillations. The number of vanadium vacancies is increasing with x, while the number of oxygen vacancies is decreasing.

MgO(004) peaks using the Bragg law. 2θ values were determined by fitting the peaks to a Gaussian function. The perpendicular lattice constant is plotted in Fig. 10 as a function of the oxygen content. We found that the perpendicular lattice constant and consequently also the average lattice constant is decreasing with increasing oxygen content. This is in contrast to the behavior reported by Banus *et al.*[6] for bulk VO_x.

The layer thicknesses determined from x-ray specular reflectivity measurements were in good agreement with the values obtained from the RHEED intensity oscillation period.

D. Vacancy concentration

As already mentioned in the Introduction, a large number of both vanadium and oxygen vacancies is characteristic for bulk VO_x. An estimation of the amount of vacancies present in VO_x thin films can be made by using a combination of RHEED and RBS results. RHEED oscillation periods were determined for all the VO_x samples as well as for a calibration V_2O_3 thin film on $Al_2O_3(0001)$. All samples were grown using the same value for the vanadium flux. By comparing the time needed to grow one monolayer of VO_x and V_2O_3, and assuming that V_2O_3 is stoichiometric and free of vacancies, the fraction of vacant vanadium sites (V_V) in VO_x can be calculated directly. The oxygen vacancy concentration (V_O) can be obtained because x is already known from RBS, using the following expression:

$$x = \frac{1 - V_O}{1 - V_V}. \tag{2}$$

As illustrated in Fig. 11, the vanadium vacancy concentration is increasing with increasing oxygen content x, while the oxygen vacancy concentration is decreasing. The total number of vacancies ($V_V + V_O$) is also decreasing with x. Close to the stoichiometric value we found about 16% vacant sites of both vanadium and oxygen.

E. Valence of the V ions from XAS

XAS measurements were done at the O K edge in order to determine the valence of the vanadium and oxygen ions. The data are depicted in Fig. 12, for samples with the oxygen content x (as determined from RBS) between 0.8 and 1.3. For comparison, we have also included the spectrum of a V_2O_3 film in the top part of the figure. The O K-edge absorption spectra correspond to dipole-allowed transitions from the O $1s$ to the O $2p$ shell, which is partially empty due to the hybridization with V $3d$ conduction-band states. The spectral structures that can be observed in the 528–534-eV photon energy range are dictated by these V $3d$ states.[32–35] For photon energies higher than 535 eV, oxygen of the MgO cap layer also starts to contribute to the XAS signal.[35]

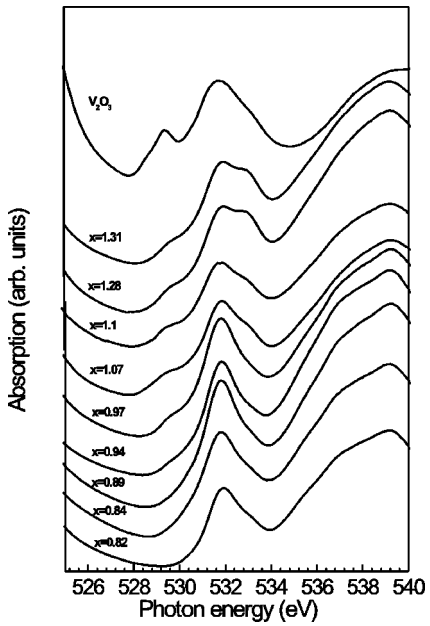

FIG. 12. O $1s$ x-ray absorption spectra of VO_x samples with the oxygen content x varying between 0.8 and 1.3.

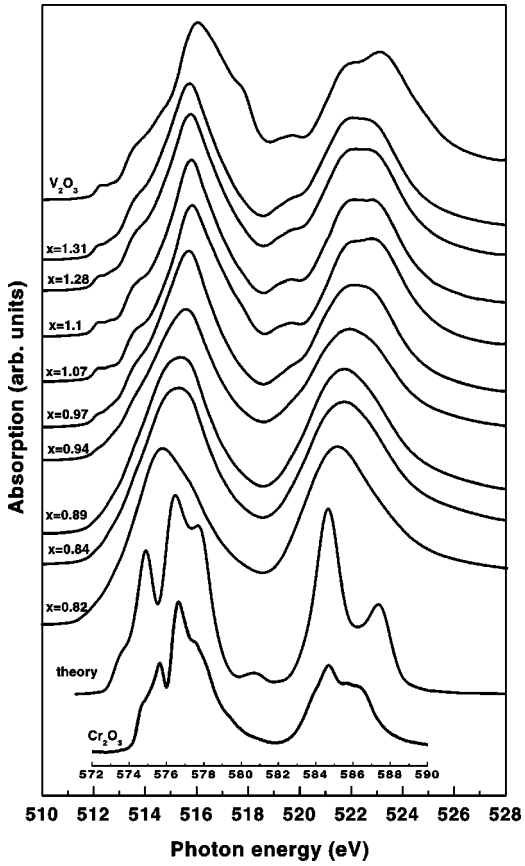

FIG. 13. V L_{23} x-ray absorption spectra of VO_x samples with the oxygen content x varying between 0.8 and 1.3.

The distinct peak observed at photon energies around 532 eV can be assigned to transitions into the empty V $3d$-$e_g{}^{\uparrow}$ band.[34] Structures at higher photon energies can be attributed to transitions to the higher-lying V $4sp$ related bands. It is important to note that for the most oxygen deficient VO_x samples, i.e., $x \ll 1$, the lowest spectral structure is given by the 532-eV peak, indicating that the lower-lying V $3d$-$t_{2g}{}^{\uparrow}$ band is completely occupied by three electrons, and that thus the V valence is $2+$ or less. For samples with higher oxygen content, i.e., $x>1$, a clear low-energy peak appears at about 530 eV. This strongly indicates that holes are introduced in the V $3d$-$t_{2g}{}^{\uparrow}$ band, meaning that the V valence is higher than $2+$. This assignment is supported by the V_2O_3 spectrum, in which transitions to both the $t_{2g}{}^{\uparrow}$ and the $e_g{}^{\uparrow}$ bands are possible because only two electrons occupy the threefold degenerate $t_{2g}{}^{\uparrow}$ orbital in this V^{3+} $3d^2$ system.

These XAS measurements show that the crossover from less than $2+$ to more than $2+$ V valencies occurs for the RBS x value of about 0.94–0.97. This value is not very far from 1.00, and can be taken as an indication of a good agreement between the XAS and RBS methods.

We also carried out XAS experiments at the V L_{23} ($2p \rightarrow 3d$) edges. The results are shown in Fig. 13. We also included in this figure the spectra of V_2O_3 and Cr_2O_3, for reference purposes. In going from $x=0.8$ to $x=1.3$, we can observe a gradual change in the spectra. Distinct and sharp structures start to develop for $x \geqslant 1$. The similarity of these structures with those of V_2O_3 is striking, and in fact indicates that V ions in a $3+$ valence state are present for $x \geqslant 1$, consistent with the observations at the O K edge mentioned above.

Important is the observation that the spectra are quite broad for x around 1. In the simplest approximation, one would expect to see a spectrum with the typical atomic multiplet structure of a $2p^6 3d^3 \rightarrow 2p^5 3d^4$ transition of a V^{2+} ion in a O_H symmetry, as shown in the bottom curve of Fig. 13. This curve has been calculated using standard parameters ($10D_q \simeq 2$ eV) often applied for the analysis of transition-metal oxide soft-x-ray-absorption spectra[36–38] and it shows quite distinct features with several peaks and valleys. Clearly, the experimental V L_{23} spectra for $x \approx 1$ do not have these distinct features.

Also, a comparison with the experimental spectrum of Cr_2O_3 (see Fig. 13), which is also a $3d^3$ ion in nearly O_H local symmetry, leads to the conclusion that the V L_{23} spectra are anomalously broad. We take this observation as an indication that vanadium in VO is not all in the local $3d^3$-O_H symmetry, but that instead an appreciable amount of vanadium ions are experiencing strong local crystal fields of low symmetry associated with the presence of large amount of vacancies. These low-symmetry crystal fields must be at least several hundreds of meV strong, in order to wash out completely the multiplet structure of a $3d^3$ ion in O_H symmetry. The implication of such fields will be discussed in Sec. IV.

F. Transport properties

Important information on the electronic structure of the VO_x system can be also obtained by investigating the electric properties. Resistivity data for polycrystalline samples of VO_x have been reported previously by Banus *et al.*[6] Bulk material exhibits a semiconducting behavior for $x>1$, with an activation energy rising to about 40 meV for $x=1.3$. For $x<1$ bulk VO_x behaves like TiO_x, with an almost temperature- and composition-independent resistivity of about 3×10^{-3} Ω cm. Banus *et al.*[6] reported a transition from a semimetallic to a semiconducting-type behavior in VO_x at $x=1.05$.

The variation of the electrical resistivity in VO_x thin films with different oxygen content is shown as a function of $1/T$ on a logarithmic scale in Fig. 14. The resistivity is increasing with decreasing T for all but the $x=0.82$ sample, suggesting a semiconductor-like behavior in the entire temperature range studied. However, it is evident in Fig. 14 that $\ln \rho$ does not vary linearly with $1/T$. Figure 15 shows the composition dependence of the activation energies calculated from the $\ln \rho$ vs $1/T$ plots close to room temperature. Note that the apparent activation energy decreases with decreasing temperature.

Such a behavior is similar to that described by Banus *et al.*[6] However, we also observed some important differences. Compared to the corresponding resistivity data for bulk samples, we found a much higher absolute value for resistivity. As can be observed from Fig. 14, the transition from a metallic- to a semiconductor-type behavior is shifted from $x=1$, as found in bulk material,[6] to $x=0.8$ for thin

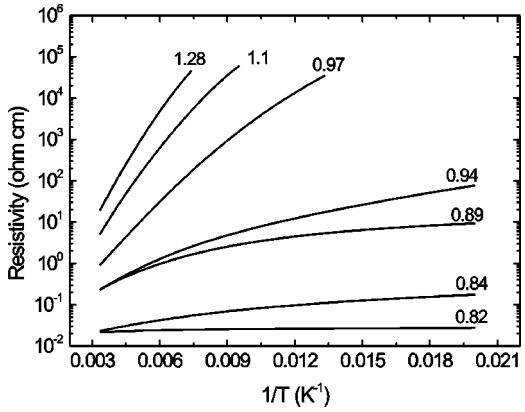

FIG. 14. Resistivity vs $1/T$ in VO_x films ($0.82<x<1.28$) plotted on a logarithmic scale. Resistivity is increasing with decreasing temperature except for the $x=0.82$ sample, suggesting a semiconductor-like behavior.

films. Moreover, the activation energy calculated close to room temperature (Fig. 15) is larger. For example, for bulk stoichiometric VO, Banus *et al.*[6] obtained an apparent activation energy of only 5 meV. For thin films we found a much higher value of ≈ 110 meV. A large increase in the activation energy can be observed in going from $x=0.94$ to $x=0.97$. Although the oxygen content is changing only by 3%, the activation energy is becoming almost twice as large. For $x\approx 1.3$ the activation energy rises to 180 meV, as compared to 40 meV in bulk.[6]

We found that T dependence of the resistivity is quite well described by variable range hopping behavior,[39] according to the following relation:

$$\rho \approx \exp\left(\frac{T_0}{T}\right)^{1/4}. \tag{3}$$

This is evident from Fig. 16, where the normalized resistivity versus $T^{-1/4}$ is plotted. This result is not surprising in view of the large number of vacancies in this material. A random field caused by vacant sites can produce localization of the electrons near the Fermi level just like in amorphous materials. Its occurrence in VO_x seems to be strong evidence

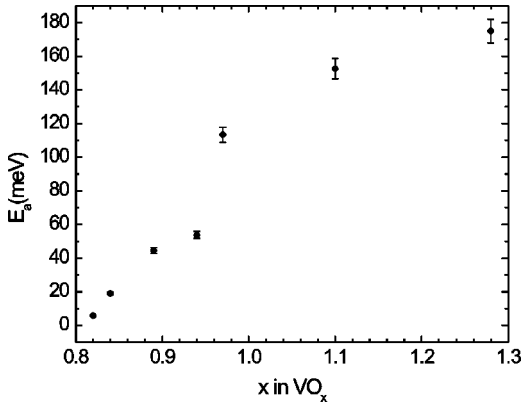

FIG. 15. Activation energy E_a vs x calculated for the temperature interval $150<T<300$ K in VO_x thin films ($0.82<x<1.28$).

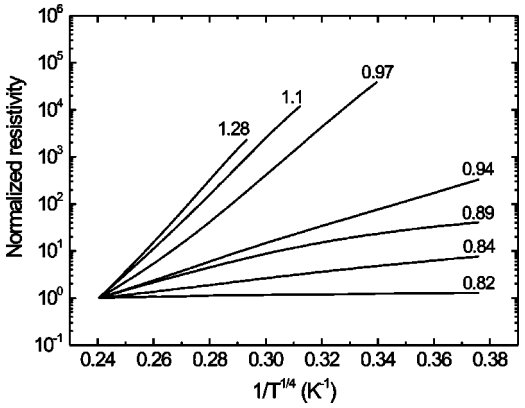

FIG. 16. Normalized resistivity in VO_x thin films ($0.82<x<1.28$) plotted as a function of $T^{-1/4}$ on a logarithmic scale.

that the vacancies play a major role, causing large changes in its electronic properties. The parameter T_0 can be extracted from the slope of the curves in Fig. 16. T_0 is related to the density of localized states at the Fermi level $N(E_F)$ by the following expression:[40]

$$T_0 = \frac{24\alpha^3}{\pi N(E_F) k_B}, \tag{4}$$

where α^{-1} is the decay length of the wave function associated with the charge carriers and k_B is the Boltzmann constant. Taking a reasonable value for α^{-1} as 5 Å,[40] $N(E_F)$ can be easily calculated from the values of T_0. These quantities are collected in Table I together with the corresponding x values. Clearly, one can observe that for the $x=0.82$ sample the density of localized states at the Fermi level is high and starts to decrease with increasing the oxygen content.

IV. DISCUSSION

The transport properties of VO_x cannot be understood on the basis of a simple band picture because the material should have been metallic. Shortly after the publication of Banus *et al.*, two theoretical papers by Goodenough[8] and Mott[9] appeared, where the electric properties of the VO_x system were explained in terms of electron correlation and vacancies. Both authors assumed a finite Hubbard U, which is large enough to split the t_{2g} band. Because V^{2+} supplies

TABLE I. Parameters extracted from $T^{-1/4}$ dependence of resistivity.

x in VO_x	T_0 (K)	$N(E_F)$ (cm^{-3} eV^{-1})
0.82	2.6	2×10^{26}
0.84	2×10^{3}	2×10^{23}
0.89	5×10^{4}	8×10^{21}
0.94	12×10^{4}	3×10^{21}
0.97	5×10^{6}	1×10^{20}
1.1	1×10^{7}	4×10^{19}
1.28	2×10^{7}	2×10^{19}

three electrons to the t_{2g} band, the valence band of VO is given by a completely filled lower Hubbard band, separated by a gap from the conduction band which is the empty upper Hubbard band.

According to Mott,[9] the random field due to the presence of vacant sites causes Anderson localization[41] in the overlap region of the two Hubbard bands. This explains why the conductivity in VO_x is of variable range hopping-type at low temperatures. In Goodenough's model[8] the effect of the vacancies on the electronic structure is discussed much more explicitly. He assumes a high degree of trapping of electron and holes near anion and cation vacancies, respectively. In this way the Fermi-level stays near the minimum in the density of states of VO_x, explaining its semiconductorlike behavior. The transition to a more itinerant behavior for $x<1$ is attributed to a tail in the trapped electron distribution. A second effect of the trapping of charges near vacancies is that the loss of Madelung energy is limited.

The presence of a large number of vacancies in VO_x remains one of the most puzzling characteristics. The only two other binary oxides showing this behavior are the rocksalts TiO_x and NbO, with NbO having about 25% vacancies.[42] Apparently the creation of vacancies stabilizes the structure by reducing the Gibbs free energy. According to Goodenough,[8] the formation of vacancies leads to a reduction in the lattice constant, thereby broadening the t_{2g} bands. The resulting stabilization of the occupied valence-band states is counteracted by a reduction in the Madelung energy, but this energy loss is assumed to be minimized by a localization of the charge compensating electrons and holes near the oxygen and vanadium vacancies, respectively. He argues that the application of hydrostatic pressure should reduce the vacancy concentration considerably and he refers to experiments giving indirect evidence in favor of this effect.[43]

The VO_x films we have grown epitaxially on MgO substrates are thin enough to be coherent with the substrate and are under tensile stress. In fact, the in-plane lattice constant is expanded by $\approx 3\%$, while the out-of-plane lattice constant is reduced due to the Poisson effect. Applying Goodenough's vacancy induced lattice contraction arguments, we would expect that the formation of vacancies will be less favored in our thin film, because the lattice constant of the film is fixed by the substrate, thus preventing the energy gain to occur, which otherwise is associated with the lattice contraction and broadening of the t_{2g} bands. In contrast with this expectation, however, we found that both cation and anion concentrations are not much affected. For a stoichiometric VO film, the values are even slightly higher (of the order of 1% or 2%) than for the bulk material.

We agree with Goodenough, nevertheless, that the mechanism for vacancy formation must be searched for in terms of energy arguments. To our knowledge, *ab initio* total-energy calculations have not yet been carried out to study the stability of vacancy formation in this material. We may speculate about the mechanism by reviewing Goodenough's arguments.[8] Goodenough assumes that electrons and holes are being trapped near cation and anion vacancies, as to avoid part of the Madelung energy loss. The t_{2g} orbitals of cations neighboring a cation vacancy are then destabilized by a reduced bonding to neighboring t_{2g} orbitals and a stronger π bonding to the p orbitals next to the vacancy, thereby raising their energy above the Fermi level. On the other hand, near an oxygen vacancy the bonding t_{2g} orbitals are stabilized, whereas the e_g and s orbitals are less destabilized by the absence of oxygen p_σ orbitals at the vacant site. These effects contribute to the stabilization energy of vacancies, but not enough. Instead of looking for a possible further energy gain in the t_{2g} band due to band broadening as a result of lattice contraction, we discuss next how ligand field effects due to the lower local symmetry in the presence of a vacant adjacent site can lower the energy of the occupied t_{2g} states. We note that the XAS measurements reveal that those ligand fields are very strong in VO_x, i.e., with a strength of the order of several hundreds meV.

We will first discuss the case of oxygen vacancies. Neighboring divalent $3d$ metal ions are surrounded by five oxygen ligands in a square pyramidal arrangement with C_{4v} symmetry. The t_{2g} and e_g levels will be split into three nondegenerate and one doubly degenerate levels, respectively. With two electrons being trapped at or near the vacancy, we have one extreme possibility where both electrons are trapped at the vacant site, forming a so-called F center. The other possibility is that the excess electrons are trapped at neighboring d-metal sites. Assuming that at least a fraction of the excess electrons resides at the adjacent d-metal ions, the average number of d electrons will be larger than three for V ions next to an oxygen vacancy. In both cases some ligand field stabilization energy is gained, owing to the electrons occupying the lower e_g level in $VO_{x<1}$.

Considering now the case of d-metal vacancies, we may speculate that two excess holes are trapped near these vacancies in $VO_{x>1}$. One extreme possibility is that the holes are residing at oxygen neighbors. Following a suggestion by Elfimov *et al.*,[44] this would give a stable configuration in which the holes are in a triplet state localized at the oxygen coordination polyhedron around the vacancy. However, in contrast with the case of CaO discussed by these authors, in a transition-metal compound there is also the possibility that the two holes are located at next-nearest-neighbor transition-metal ions. The presence of the cation vacancy leads to a local-symmetry lowering (C_{2v}) at these cation sites. Also in this case a ligand field stabilization is anticipated, because the average number of d electrons on d-metal ions next to a vacancy will be less than 3 per V ion.

As argued above, although the decrease of direct overlap between t_{2g} orbitals in the strained films does not have a major effect on the concentration of vacancies, it will change the valence-band structure and consequently change the electrical properties. Expanding the lattice by epitaxial growth on a substrate with a larger lattice constant such as MgO will decrease the bandwidth and therefore increase the gap. This explains the lower conductivity and higher room-temperature activation energies found in our films. In the models proposed by Goodenough[8] and Mott,[9] the on-site Coulomb interaction U is assumed to open up a small energy gap in the itinerant t_{2g} band. It is assumed that overlapping tails of localized states, which are related to the disorder associated with the large number of defects in the system, are present at

the edges of these Hubbard bands. In this way Mott[9] explains why in bulk samples the conductivity versus temperature dependence is semiconductorlike at high temperatures, but is better described by a variable range hopping mechanism at low temperatures. The conductivity data for our films are consistent with this explanation. The main difference is that the resistivity and apparent activation energies of the films are much higher. Also, the transition from semiconducting to metallic behavior is shifted to lower x values, i.e., from $x \approx 1$ in bulk samples to $x \approx 0.8$ in films.

V. CONCLUSIONS

We have successfully grown epitaxial VO_x films on MgO(100) substrates. Up to at least 120 Å, the growth is coherent and layer-by-layer-like. $^{18}O_2$ RBS was introduced as a convenient method to determine accurately the stoichiometry of these ultrathin layers. Once the stoichiometry is known, the vacancy concentration of both vanadium and oxygen can be calculated from the time required to grow one monolayer as determined from RHEED. The numbers turn out to be very similar to those for the bulk material. This implies that the formation of a high concentration of vacancies may not be directly related to an increased t_{2g} bandwidth as a result of a vacancy-induced lattice contraction. Instead we think that a detailed study is required in order to calculate the possible stabilization due to additional ligand field effects induced by the local-symmetry lowering at metal sites near the vacancy, as observed from XAS. Nevertheless, the decrease in direct overlap between t_{2g} orbitals and the concomitant increase of the size of the pseudogap between the lower and upper t_{2g} Hubbard bands is held responsible for the much larger electrical resistivity in strained VO_x films.

ACKNOWLEDGMENTS

We would like to thank D. I. Khomskii, T. T. M. Palstra, and D. O. Boerma for stimulating discussions, as well as H. Bruinenberg and J. Baas for skillful technical assistance. We would like to thank A. Tanaka for the use of the code to calculate the XAS spectra. The research of M.W.H. and L.H.T. was supported by the Deutsche Forschungsgemeinschaft through SFB 608.

[1] J.B. Goodenough, *Magnetism and the Chemical Bond* (Wiley, New York, 1963).
[2] W. Brückner, H. Oppermann, W. Reichelt, J.I. Terukow, F.A. Tschudnowski, and E. Wolf, *Vanadiumoxide* (Akademie-Verlag, Berlin, 1983).
[3] N. Tsuda, K. Nasu, A. Fujimori, and K. Siratori, *Electronic Conduction in Oxides* (Springer-Verlag, Berlin, 2000).
[4] M. Imada, A. Fujimori, and Y. Tokura, Rev. Mod. Phys. **70**, 1039 (1998).
[5] C.N.R. Rao and B. Raveau, *Transition Metal Oxides* (Wiley-VCH, New York, 1998).
[6] M.D. Banus, T.B. Reed, and A.J. Strauss, Phys. Rev. B **5**, 2775 (1972).
[7] M. Morinaga and J.B. Cohen, Acta Crystallogr., Sect. A: Cryst. Phys., Diffr., Theor. Gen. Crystallogr. **35**, 745 (1979).
[8] J.B. Goodenough, Phys. Rev. B **5**, 2764 (1972).
[9] N.F. Mott, Philos. Mag. **24**, 935 (1971).
[10] P.A. Cox, *Transition Metal Oxides* (Oxford University Press, Oxford, 1995).
[11] A. Neckel, P. Rastl, R. Eibler, P. Weinberger, and K. Schwarz, J. Phys. C **9**, 579 (1976).
[12] K. Kishi, K. Hirai, and T. Yamamoto, Surf. Sci. **290**, 309 (1993).
[13] K. Kishi, Y. Hayakawa, and K. Fujiwara, Surf. Sci. **356**, 171 (1996).
[14] K. Kishi and K. Fujiwara, J. Electron Spectrosc. Relat. Phenom. **85**, 123 (1997).
[15] T. Hartmann and H. Knozinger, Z. Phys. Chem. (Munich) **197**, 113 (1996).
[16] F.P. Leisenberger, S. Surnev, L. Vitali, M.G. Ramsey, and F.P. Netzer, J. Vac. Sci. Technol. A **17**, 1743 (1999).
[17] S. Surnev, L. Vitali, M.G. Ramsey, and F.P. Netzer, Phys. Rev. B **61**, 13 945 (2000).
[18] V.E. Henrich and P.A. Cox, *The Surface Science of Metal Oxides* (Cambridge University Press, Cambridge, 1994).
[19] M.D. Negra, M. Sambi, and G. Granozzi, Surf. Sci. **436**, 227 (1999).
[20] M.D. Negra, M. Sambi, and G. Granozzi, Surf. Sci. **461**, 118 (2000).
[21] M. Sambi, M.D. Negra, and G. Granozzi, Thin Solid Films **400**, 26 (2001).
[22] F.C. Voogt, T. Fujii, M.A. James, and T. Hibma, Phys. Rev. B **63**, 125409 (2001).
[23] M.A. James, F.C. Voogt, B. Niesen, O.C. Rogojanu, and T. Hibma, Surf. Sci. **402-404**, 332 (1998).
[24] M.A. James and T. Hibma, Surf. Sci. **433-435**, 718 (1999).
[25] H. Schuler, S. Klimm, G. Weissmann, C. Renner, and S. Horn, Thin Solid Films **299**, 119 (1997).
[26] H. Schuler, G. Weissmann, C. Renner, S. Six, S. Klimm, F. Simmet, and S. Horn, in *Epitaxial Oxide Thin Films II*, edited by D. K. Fork *et al.*, MRS Symposia Proceedings No. 401 (Materials Research Society, Pittsburgh, 1996), p. 61.
[27] H. Schuler, S. Grigoriev, and S. Horn, in *Epitaxial Oxide Thin Films III*, edited by D. G. Schlom, MRS Symposia Proceedings No. 474 (Materials Research Society, Pittsburgh, 1997), p. 291.
[28] C.T. Chen, Nucl. Instrum. Methods Phys. Res. A **256**, 595 (1987).
[29] C.T. Chen and F. Sette, Rev. Sci. Instrum. **60**, 1616 (1989).
[30] S.A. Chambers, Surf. Sci. Rep. **39**, 105 (2000).
[31] G. Sawatzky and D. Post, Phys. Rev. B **20**, 1546 (1979).
[32] M. Abbate, H. Pen, M.T. Czyzyk, F.M.F. de Groot, F.C. Fuggle, Y.J. Ma, C.T. Chen, F. Sette, A. Fujimori, Y. Ueda, and K. Kosuge, J. Electron Spectrosc. Relat. Phenom. **62**, 185 (1993).
[33] F.M.F. de Groot, M. Grioni, F.C. Fuggle, J. Ghijsen, G.A. Sawatzky, and H. Petersen, Phys. Rev. B **40**, 5715 (1989).
[34] J. van Elp and Arata Tanaka, Phys. Rev. B **60**, 5331 (1999).
[35] S. Nakai, T. Mitsuishi, H. Sugawara, H. Maezawa, T. Matsukawa, S. Mitani, K. Yamasaki, and T. Fujikawa, Phys. Rev. B **36**, 9241 (1987).

[36] See review by F.M.F. de Groot, J. Electron Spectrosc. Relat. Phenom. **67**, 529 (1994).
[37] See review in the Theo Thole Memorial Issue, J. Electron Spectrosc. Relat. Phenom. **86**, 1 (1997).
[38] A. Tanaka and T. Jo, J. Phys. Soc. Jpn. **63**, 2788 (1994).
[39] N. Mott, *Metal-Insulator Transitions* (Taylor & Francis, London, 1990).
[40] A.R. Brown, C.P. Jarrett, D.M. de Leeuw, and M. Matters, Synth. Met. **88**, 37 (1997).
[41] P.W. Anderson and H. Hasagawa, Phys. Rev. **100**, 675 (1958).
[42] H. Erschbaumer, R. Podloucky, and A. Neckel, J. Phys. F: Met. Phys. **15**, L279 (1985).
[43] M.D. Banus, Mater. Res. Bull. **3**, 723 (1968).
[44] I.S. Elfimov, S. Yunoki, and G.A. Sawatzky, Phys. Rev. Lett. **89** **89**, 216403 (2002).